Tritiated amorphous silicon betavoltaic devices

T. Kosteski, N.P. Kherani, P. Stradins, F. Gaspari, W.T. Shmayda, L.S. Sidhu and S. Zukotynski

Abstract: The introduction of tritium into hydrogenated amorphous silicon has given rise to a novel material with interesting physical properties and potential applications. Tritium undergoes radioactive decay, transforming into $^3He^+$ and emitting an electron with average energy 5.7 keV, at a rate equivalent to a half-life of 12.3 years. The decay of tritium results in the creation of electron–hole pairs and in the formation of dangling bonds. Infrared spectroscopy and effusion measurements were used to analyse tritium bonding in the silicon network. Electron spin resonance and photoluminescence of tritiated amorphous silicon were examined as a function of time to study the evolution of dangling bonds. Thermal annealing was used to study metastability of dangling bonds in the material. Electrical characteristics of pin diodes containing tritium in the intrinsic layer were investigated. The application of tritiated–hydrogenated amorphous silicon in betavoltaic devices is presented.

1 Introduction

Hydrogenated amorphous silicon (a-Si:H) is an amorphous semiconductor whose optoelectronic properties, combined with its relatively low cost of fabrication, have made it an established material in semiconductor technology, particularly for photovoltaics and active matrix displays [1, 2].

When prepared by conventional evaporation or sputtering, amorphous silicon contains a large concentration of defects and microvoids [3, 4]. These give rise to localised states in the energy gap of the material [3, 4]. Plasma-enhanced chemical vapour deposition (PECVD), using silicon hydrides, significantly reduces the number of defects and thereby lowers the concentration of localised states in the energy gap [3–5]. It is well known that hydrogen is responsible for defect passivation [3–5]. Hydrogen atoms incorporated into the films satisfy the covalent bonds at defects and microvoids and also allow the lattice to relax, thereby reducing the density of localised states by several orders of magnitude [3–5].

Tritium (T) is an isotope of hydrogen and is expected to readily replace hydrogen in a-Si:H [6]. Tritium is radioactive and undergoes beta decay according to the following reaction:

$$^3H \rightarrow {}^3He^+ + \beta^- + \bar{\nu} \qquad (1)$$

where β^- is a beta particle and $\bar{\nu}$ is an antineutrino. The antineutrino is essentially undetectable; thus tritium is considered to be a pure beta emitter. The half-life of tritium is 12.3 years, or equivalently the decay rate of tritium is $1.78 \times 10^{-9}\,s^{-1}$. Accordingly, 1 cm^3 of tritium at standard temperature and pressure has an activity of 2.6 Ci. The kinetic energy spectrum of beta-particles produced from the decay of tritium is shown in Fig. 1 [7]. The maximum energy of the beta-particles is 18.6 keV while the average energy is 5.7 keV. Considering the energy distribution, the power available from the kinetic energy of the beta-particles is 33.7 μW/Ci.

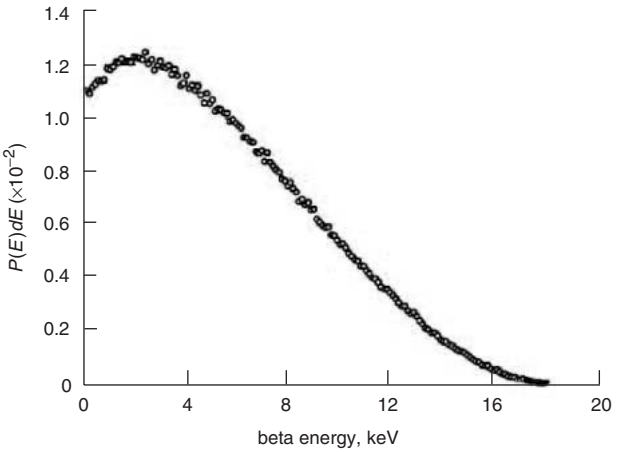

Fig. 1 *Kinetic energy spectrum of beta-particles produced from the decay of tritium [7] dE = 0.112 keV*

For 1 at.% of tritium in silicon, the power released in a 1 μm film of tritiated amorphous silicon (a-Si:H:T) is 0.08 $\mu W/cm^2$. The average range of a 5.7 keV beta-particle in silicon is 0.2 μm [8]; thus most of this power is trapped in the film. The incorporation of tritium into a-Si:H is expected to give rise to a family of devices in which the energy output of the radioactive process of tritium decay is integrated with the optoelectronic properties of a-Si:H.

2 Deposition of tritiated amorphous silicon

A schematic of the saddle-field glow discharge facility for the preparation of tritiated amorphous silicon is shown in Fig. 2 [9, 10]. The deposition chamber is outfitted with three

IEE Proceedings online no. 20030628

doi:10.1049/ip-cds:20030628

Paper first received 5th February and in revised form 19th May 2003

T. Kosteski, N.P. Kherani, F. Gaspari and S. Zukotynski are with the Department of Electrical and Computer Engineering, University of Toronto, 10 King's College Road, Toronto, Ontario, Canada M5S 3G4

P. Stradins is with the National Renewable Energy Laboratory, 1617 Cole Boulevard, Golden, CO 80401-3393, USA

W.T. Shmayda is with the Laboratory for Laser Energetics, University of Rochester, 250 East River Road, Rochester, NY 14623-1299, USA

L.S. Sidhu was with the University of Waterloo, Canada and is now with the Altera Corporation, 101 Innovation Drive, San Jose, CA 95134, USA

Table 1: Deposition conditions of samples

	Deposition B	Deposition C	Deposition D
Gas flow	2.5 sccm SiH_4	2.5 sccm SiH_4	2.5 sccm SiH_4
	2.5 sccm T_2	2.5 sccm T_2	2.5 sccm T_2
Pressure	50 mtorr	50 mtorr	50 mtorr
Anode potential	610 to 650 V	580 to 620 V	1010 to 1120 V[a]
			590 to 600 V[b]
Anode current	4 mA	30 mA	22 to 24 mA[a]
			30 mA[b]
Substrate potential	Ground	Ground	Floating 350 V[a], 280 V[b]
Substrate current	0.4 mA	7 to 8 mA	—
Substrate temperature	225°C	150°C	150°C
Samples described in this paper	A69	A155, A170, G181	A206, A212, A214

[a] During the first half of deposition.
[b] During the second half of deposition.

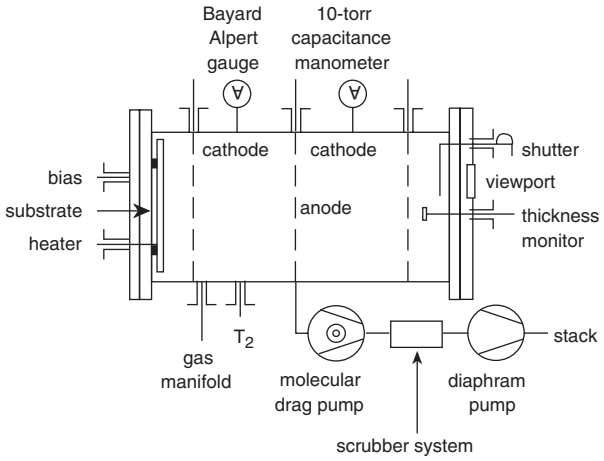

Fig. 2 *Saddle-field glow discharge apparatus for the preparation of tritiated amorphous semiconductors*

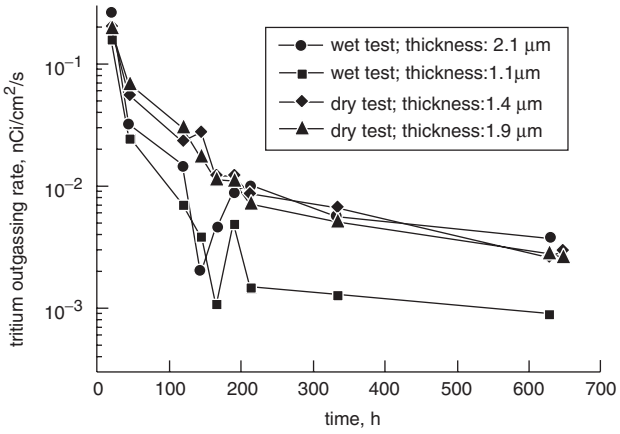

Fig. 3 *Outgassing rate from four a-Si:H:T films from deposition D (see Table 1)*

coarse stainless steel mesh electrodes, as shown. A glow discharge is created between the central electrode (the anode) and the outer two electrodes (the cathodes). A heated, electrically isolated substrate holder is mounted in the chamber. The substrate holder can be electrically biased.

Silane, diborane, and phosphine are available through a common port on the chamber. Tritium, which is stored as a tritide on a depleted uranium bed, is available through another port on the chamber. Each gas source is equipped with a mass-flow controller to permit independent control of flow. Evacuation of the deposition facility is provided by an oil-free system, which consists of a molecular drag pump and a diaphragm pump. A scrubber system, positioned between the two vacuum pumps, is used to strip tritium from the chamber effluent. The deposition system is housed in a nitrogen-atmosphere glovebox.

The deposition conditions of the single-layer films discussed in this paper are listed in Table 1.

3 Tritium outgassing

The rate of tritium outgassing, at room temperature, from as-deposited tritiated amorphous silicon films [5 to 10 at. % of tritium, as measured by infrared spectroscopy (see Section 5)] was estimated by measuring the evolution of tritiated water from a number of a-Si:H:T samples under dry and wet or humid air ambient [Note 1]. Experimental results show that after approximately 600 h of outgassing, the total quantity of tritium desorbed from each of the samples is less than 40 μCi cm^{-2}. The cumulative tritium desorption under dry and wet conditions is of the same order of magnitude. This suggests that to first order, HTO is the predominant desorbing species. The rate of tritium outgassing for four samples at room temperature is shown in Fig. 3. The rate of outgassing is comparable for samples in dry and wet atmospheres. The a-Si:H:T samples show an initial outgassing rate of the order of 200 pCi cm^{-2} s^{-1}. After about 600 h of outgassing, the tritium outgassing rate appears to approach a value of less than 10 pCi cm^{-2} s^{-1} or less than 1 part in 10^9 s^{-1} from a 1 μm film with 5 at.% of tritium. This suggests that the source of the outgassing tritium is the top few monolayers of the film.

4 Effusion of tritium

Samples of a-Si:H:T were subjected to linear temperature ramping from room temperature to approximately 900°C in an argon purge. The experimental setup for tritium effusion measurements is described elsewhere [11]. The effusion

Note 1: As described in a paper being prepared for submission (Kherani, N.P., Virk, K., Kosteki, T., Gaspari, F., Shmayda, W.T., and Zukotynski, S.: 'Hydrogen effusion from tritiated amorphous silicon')

experiments were carried out at temperature ramp rates of 5, 10, 20, and 40°C/min. The tritium evolution data for two samples grown at two different substrate temperatures are shown in Figs. 4 and 5. The thickness of the samples was ~0.8 μm for sample A155 (Fig. 4) and ~0.2 μm for sample A212 (Fig. 5).

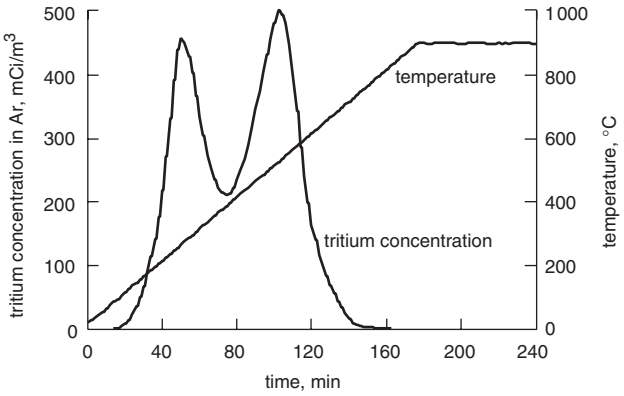

Fig. 4 *Tritium evolution from an a-Si:H:T film (A155) grown at 150°C*

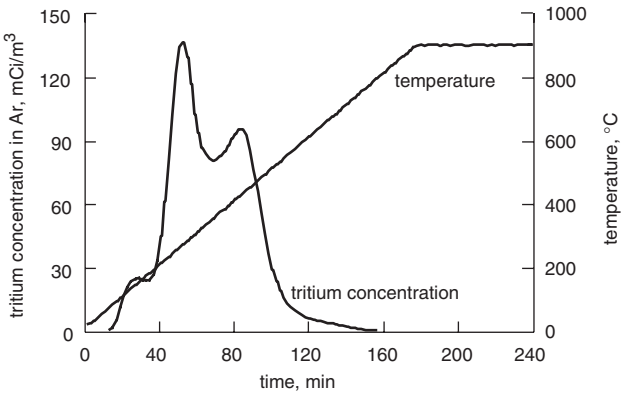

Fig. 5 *Tritium evolution from an a-Si:H:T film (A69) grown at 225°C*

It can be seen that significant tritium evolution occurs only when the sample temperature exceeds the growth temperature. At temperatures below the growth temperature but above room temperature there is an increase in the tritium monitor signal, which is equivalent to a tritium concentration change of $100\,\mu Ci\,m^{-3}$ in a volume of 1 l. This evolution is mainly due to surface tritium and represents a surface tritium concentration of about $10\,\mu Ci\,cm^{-2}$; this is of the same order of magnitude as that measured in the outgassing experiments presented above ($40\,\mu Ci\,cm^{-2}$). Alternatively, the total number of hydrogen atoms on the surface can be estimated to be $6 \times 10^{14}\,cm^{-2}$. To put this number in context, the number of silicon atoms constituting a monolayer is about $10^{15}\,cm^{-2}$. Considering that the total atomic hydrogen content in these films is around 15 to 30 at.%, the foregoing numbers suggest that the surface hydrogen originates from the top two to three monolayers of the sample. Typical effusion profiles in Figs. 4 and 5 clearly show the presence of several peaks that are suggestive of different hydrogen–silicon binding states.

5 Infrared spectroscopy

To investigate the bonding of tritium in the amorphous silicon network, we compared the infrared spectra of a hydrogenated (a-Si:H), a deuterated (a-Si:H:D), and a tritiated (a-Si:H:T) film of similar thickness (0. 2 to 0.3 μm). Figure 6 shows the high-frequency part of the spectra for the three films, with the individual curves shifted vertically with respect to each other by approximately $500\,cm^{-1}$, for clarity. The vibrations near $2000\,cm^{-1}$ in the a-Si:H film indicates Si–H stretching modes [12]. Very similar hydrogen peaks are observed in the a-Si:H:D and a-Si:H:T films, the hydrogen originating from the silane gas. The deuterated and tritiated spectra show additional peaks near $1500\,cm^{-1}$ and $1200\,cm^{-1}$, respectively. These peaks are attributed to Si–D and Si–T stretching vibrations. The greater-reduced mass of the Si–D and Si–T oscillators relative to that of the Si–H oscillator is responsible for the shift to lower frequencies. The integrated area of the Si–T stretching mode was used to determine the tritium content [13].

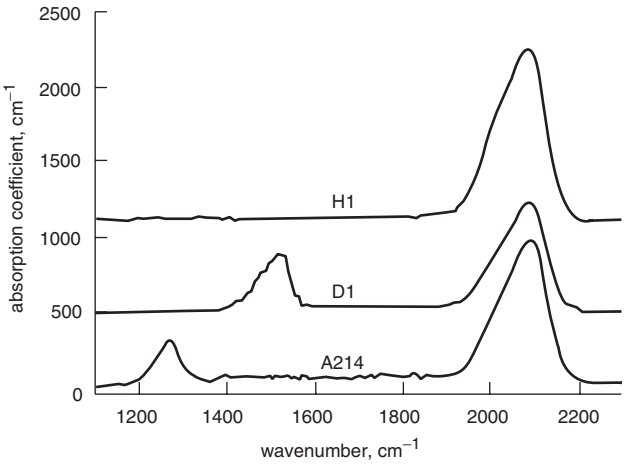

Fig. 6 *High-frequency IR vibrations of hydrogenated (H1), deuterated (D1), and tritiated (A214) amorphous silicon films*
D1 and H1 have been shifted with respect to A214 for clarity

Using the harmonic potential approximation, the stretching frequencies of the Si–D(T) bonds can be calculated with respect to the Si–H bond stretching frequency, i.e.

$$\frac{\omega_{i-D(T)}}{\omega_{Si-H}} = \sqrt{\frac{m_H(m_{D(T)} + M_{Si})}{m_{D(T)}(m_H + M_{Si})}} \qquad (2)$$

where, $\omega_{Si-H(D,T)}$ is the stretching frequency of the Si–H(D,T) bond, $m_{H(D,T)}$ denotes the mass of hydrogen (deuterium, tritium), and M_{Si} represents the mass of silicon. Table 2 tabulates the experimental and calculated ratios.

Table 2: Ratio of stretching frequency of Si–D and Si–T bonds with respect to Si–H bonds

Ratio of frequencies	Experimental	Calculated
$\omega_{Si-D}/\omega_{Si-H}$	0.73	0.72
$\omega_{Si-T}/\omega_{Si-H}$	0.61	0.60

The weak integrated intensity of the deuterium- and tritium-related vibrations, relative to that of hydrogen absorption bands is expected since integrated intensity is inversely proportional to the reduced mass of the oscillator. An analysis of the lower frequency modes (wagging, bending, etc.) leads to similar agreement between experimental and calculated values [13]. This confirms that both deuterium and tritium behave as heavy hydrogen atoms in

the amorphous silicon network and establish a similar bonding pattern.

6 Dangling bonds in a-Si:H:T

When beta decay of tritium in a-Si:H:T occurs, a high-energy electron is released and the tritium nucleus transmutates into helium. The following processes take place in the material:

(i) The beta-particles created in the process of radioactive decay interact with the amorphous network and generate over 1000 electron–hole (e–h) pairs each [10]. The energy of the beta-particle is insufficient, however, to cause irreversible lattice damage [14, 15].

(ii) The recoil energy of the helium is about 3 eV, which is insufficient to cause irreversible lattice damage [15, 16].

(iii) Helium does not stably bond with silicon; therefore, a silicon dangling bond is created at the site of each decayed tritium atom.

The rate of dangling bond formation due to bonded tritium decay is

$$\frac{dN_{db}(t)}{dt} = \lambda N_T \exp(-\lambda t) \quad (3)$$

where N_{db} is the concentration of dangling bonds, N_T is the tritium concentration at $t=0$ and λ is the decay rate of tritium.

Initially, the dangling bonds must be positively charged (D^+ centres); however, with time, the D^+ centres are expected to attract electrons and be converted into neutral dangling bonds (D^0 centres). This process should have a high probability due to the large number of free electrons present in the material. To stabilise the transition from a D^+ to D^0 centre, however, a 15° bond-angle change is necessary [17]. This reduces the probability of the conversion; consequently, we expect that re-emission of electrons will compete with the D^+ to D^0 conversion process and a steady concentration of D^+ and D^0 centres will develop, determined by the tritium decay and the electron re-emission process.

We investigated the formation of dangling bonds using electron spin resonance and photoluminescence.

7 Electron spin resonance

Electron spin resonance (ESR) provides a direct measurement of the concentration of Si dangling bond D^0 neutral defect states [18]. We have monitored concentrations of defects and studied their time evolution and annealing behaviour in sample G181 (~1.5 μm thick) using a Bruker ESR spectrometer. Just after deposition, the tritium and hydrogen concentrations were 9 at.% and 22 at.%, respectively. The spin resonance was first measured after 4 years of storage. Due to the ongoing decay of tritium to helium one would expect the Si dangling bond defect concentration to be as high as $N_{db} = 5 \times 10^{21}\,cm^{-3}$ at the time of the ESR measurement. An additional degradation effect by emitted beta-particles, if any, would make this concentration even higher. Surprisingly, however, the measured defect spin density was only $N_d = 6.4 \times 10^{17}\,cm^{-3}$. Such a large discrepancy suggests that there is an ongoing process that either eliminates the created defects or makes them invisible to ESR. The latter implies creation of large numbers of charged defects, D^+ and D^-.

The neutral defects observed by ESR are not stable: they anneal out by heating at 150°C. This strongly suggests that their creation is likely counterweighted by an annealing process that takes place even at room temperature. As a result, defect density finally saturates at concentrations much lower than those of the decayed tritium atoms. This annealing is somewhat similar to the thermal decay of the Si dangling bond defects created by light (Staebler–Wronski effect [19]). In the latter case, typical annealing temperatures are above 150°C, while some of the defects do anneal even at room temperature due to their very broad spectrum of annealing activation energies [20, 21]. The experimental evidence for the thermal annealing of defects in tritiated a-Si is outlined below.

After the ESR measurement, the 4-year-old a-Si:H:T sample was annealed at 150°C for 30 min and then rapidly cooled down to room temperature; the evolution of the ESR signal with time was subsequently monitored. The results are shown in Fig. 7. Annealing reduced the spin concentration to $5.6 \times 10^{16}\,cm^{-3}$. After the annealing, the spin density increased rapidly, with an initial rate of creation of defect spins roughly equal to the rate of tritium decay (dashed line). After about 20 h, however, the rate of creation of spin states slowed down considerably and the spin density again saturated at the old value of about $6 \times 10^{17}\,cm^{-3}$ within one month. We have fitted this time evolution N_d by a stretched exponential dependence:

$$N_d(t) = N_0 + (N_{sat} - N_0) \times \{1 - \exp[(-t/\tau)^{\alpha}]\} \quad (4)$$

where N_0 is the dangling bond density at $t=0$. The saturation value N_{sat} is approximately equal to the concentration of spin states measured after 4 years of storage, prior to annealing. Such dependence generally describes relaxation phenomena with time-dependent transition rates in disordered systems, including hydrogenated amorphous silicon [3, 17, 22, 23]. The time constant τ of (4) characterises, approximately, the lifetime of newly created, defects and is about 12 days at room temperature. The thermal character of the defect equilibration was further confirmed by keeping the sample at an elevated temperature of 80°C after annealing. In this case, the defect concentration saturated in less than 1 day and the saturation value was below $10^{17}\,cm^{-3}$. Such an effective annealing may be a result of very high concentrations of hydrogen and tritium in the sample, leading to clustered hydrogen regions. Experiments on samples with lower H content are being planned. It is also a challenge to explain the annealing mechanism for the defects since the concentrations of the

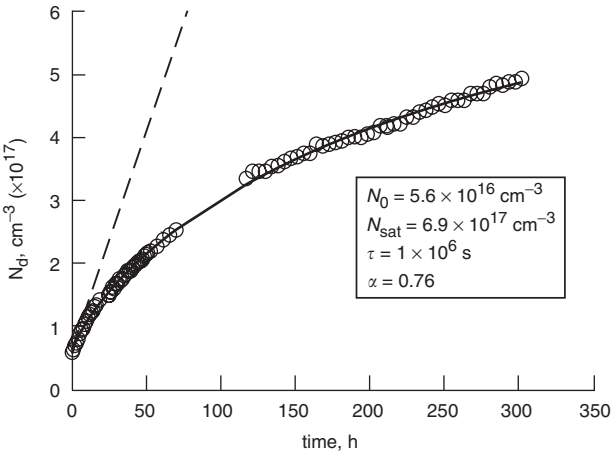

Fig. 7 *ESR results for sample G181 after 30 min annealing at 150°C*

The solid curve is a fit to the data using (4). Values of the parameters obtained from the fit are indicated in the Figure. The dashed line represents the number of tritium decays calculated using (3)

decayed tritium atoms after 4 years of sample storage are very high – of the order $10^{21}\,cm^{-3}$. One might assume that H atoms that diffuse from nearby sites annihilate these defects. In this case, H detachment from such a site should not be accompanied by the creation of a new defect. This might be possible if H comes from a large reservoir of paired H sites such as double-hydrogen complexes [24] or hydrogenated vacancies [25]. Further experiments are necessary to elucidate the mechanism of defect annealing.

8 Photoluminescence

Photoluminescence (PL) of the films was measured using an Ar^+ ion laser tuned to 490 nm. Shortly after deposition, the tritiated samples exhibited strong, low-temperature PL. The PL spectrum at 5 h after deposition and its temperature dependence were similar to those observed in samples deposited under similar conditions except for hydrogen or deuterium in place of tritium in the feed gas stream. This confirms that the density-of-states (DOS) distribution in the films does not depend strongly on the hydrogen isotope used in the feed gas stream. However, the PL of the tritiated samples decreases quickly with time, due to the creation of dangling bonds that act as recombination centres for the e–h pairs, thus quenching the luminescence signal [17].

In Fig. 8 the decay of the photoluminescence is plotted as a function of time for the three successive annealing cycles of sample A206 ($\sim$0.2 μm thick). Samples were annealed at 150°C for 30 min for each cycle. The data for the initial photoluminescence decay, immediately following deposition, for sample A170 ($\sim$0.6 μm thick) are also included in the figure. It is seen to be similar to the data for sample A206. Neutral dangling bonds (D^0) are the most effective recombination centres for e–h pairs [16] and are therefore the most likely cause of the quenching of the PL signal. The solid line in Fig. 8 is based on the theoretical model of Sidhu *et al.* [26]. According to Sidhu's model, the PL efficiency η can be written as

$$\eta = \frac{1}{1 + \tau v \exp\left[-\frac{2}{R}\left(\frac{4\pi}{3}N_d\right)^{-1/3}\right]} \qquad (5)$$

where v is the attempt-to-hop frequency, τ is the radiative lifetime, R is the tunnelling radius, and N_d is the density of neutral dangling bonds obtained from ESR measurements.

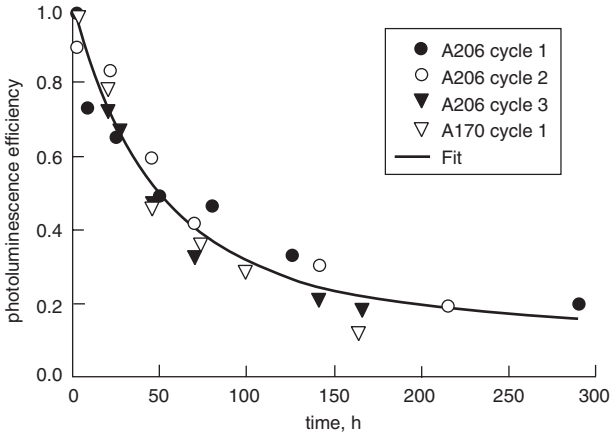

Fig. 8 *PL efficiency against time for samples A206 (three cycles) and A170 (one cycle)*
The points represent the area of the normalised PL signals. The solid line was obtained from the model developed by Sidhu *et al.* [26]

Table 3 presents the values of the parameters obtained from the fit and the expected range for these parameters.

Table 3: Measured and expected values for the parameters in (5)

Parameter	Fitted value	Expected range [3, 4, 27–29]
R	2.9 nm	1.3 to 10 nm
$v\tau$	1150	$v \sim 10^{11}$–$10^{13}\,s^{-1}$, $\tau \sim 10^{-8}$–10^{-9} s

The column labelled 'Fitted value' uses (4) in the Sidhu model. The expected range of values are from the literature

It should be noted that in an earlier paper [26] we attributed the decrease in the PL signal entirely to primary dangling bonds created through tritium decay. Over 50% of the PL decrease occurs during the first 30 h after annealing, where $D^+ \approx D^0$. Later D^+ and D^0 diverge; however, the difference in the predicted PL signal is relatively small since the concentration of dangling bonds is quite high after the first 30 h.

9 Betavoltaics

Our intrinsic betavoltaic device consists of a tritiated amorphous semiconductor p-i-n junction. The beta-induced electron–hole pairs are separated by the electric field present in the depletion region of the junction. This is similar to conventional betavoltaic or photovoltaic cells except that it is powered by intrinsic tritium decay betas rather than external electrons or external photons, respectively. A schematic illustrating the intrinsic betavoltaic device is shown in Fig. 9.

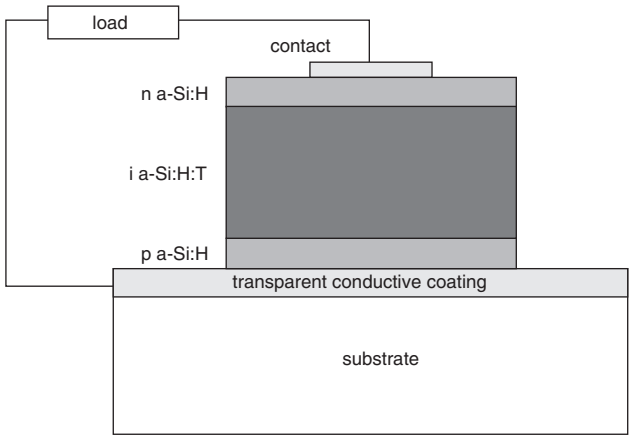

Fig. 9 *Intrinsic betavoltaic device*

The maximum power density P_{max} for this configuration was calculated to be $P_{max} = 0.29\,\mu W\,cm^{-2}$ (per $48\,mCi\,cm^{-2}$ per μm at 20 at.% tritium) [9]. Alternatively, stacking a number of such cells in series and/or in parallel would require approximately 330 Ci to achieve a 1 mW tritium powered battery. A 1 mW battery is defined as that having this power output at the end of one tritium half-life, i.e. approximately 12 years; tacit in this definition is that the cell power output diminishes at a rate equal to the decay of tritium atoms.

As described in the previous Sections, however, tritium decay creates dangling bonds. When the density of dangling bonds increases, a nonuniform electric field develops in the intrinsic region of the p-i-n junction and the effective width of the space charge region is reduced [30]. The reduced

electric field near the middle of the intrinsic region reduces the velocity of carriers and thereby increases the probability of electron–hole pair recombination. This in turn reduces the number of electron–hole pairs available for electrical power, and the output power from the betavoltaic device decreases.

As discussed earlier, dangling bonds are inevitably created as a consequence of the radioactive decay of the bonded tritium. Fortunately, the effect of these dangling bonds on the betavoltaic device can be reduced by confining the tritium to small regions of the otherwise hydrogenated amorphous silicon intrinsic region. We used a thin slice of tritiated material and refer to this as a 'delta' layer configuration. Now, rather than the entire intrinsic region being comprised of dangling bonds, only a fraction of it will contain a large concentration of dangling bonds. As a result, a uniform electric field will exist across most of the intrinsic region, and degradation of the betavoltaic device will be limited.

A p-i-n delta layer device is illustrated in Fig. 10. The p- and n-layers of the p-i-n delta layer devices were deposited using a 2% gas mixture of B_2H_6 in SiH_4 and PH_3 in SiH_4, respectively. The thickness of the p-layer was approximately 120 Å, while the thickness of the n-layer was approximately 200 Å. The hydrogenated portions of the intrinsic region for the devices were grown using undiluted SiH_4 and the thickness was approximately 0.12 μm. The tritiated delta layer was deposited using tritium gas and SiH_4. These gasses were introduced into the plasma at equal gas-flow rates of 4 sccm. The deposition time was used to control the thickness of the delta region. The total chamber pressure was maintained at 140 mtorr for the entire intrinsic region. The substrate temperature for all layers was 250°C. The anode voltage during deposition of the layers was approximately 620 V while the anode current was approximately 12 mA.

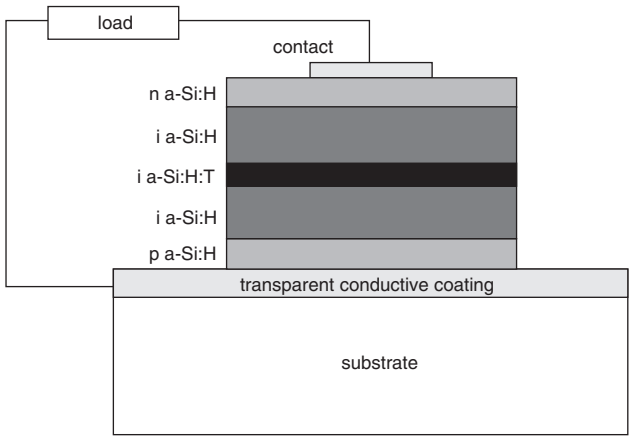

Fig. 10 *p-i-n delta layer device*

The behaviour of devices with a delta layer was compared with a device whose entire intrinsic region was tritiated. We label this last device 'uniform' while the three devices with a delta layer were labelled 'delta' 1, 2, and 3. The thickness of the tritiated layer in 'delta' 1 was approximately 1/3 of the thickness of the intrinsic layer in the device 'uniform'. Similarly, the thicknesses of the a-Si:H:T layer in delta 2 and delta 3 were approximately 1/6 and 1/12 of the thickness of the intrinsic layer in the device uniform, respectively. The concentration of tritium in the tritiated region of all devices was similar at about 5 at.%. Table 4 gives the short-circuit current and open-circuit voltage for the four devices, measured shortly after their manufacture.

Table 4: Short-circuit current and open-circuit voltage for the 'delta' devices and the device 'uniform'

Device	I_{sc} (nA) ± 2%	V_{oc} (mV) ± 0.02%
uniform	0.98	21
delta 1	0.35	20
delta 2	0.14	9
delta 3	0.03	11

Of the four devices listed in Table 4, the device 'uniform' has the largest short-circuit current. On the whole, the differences in the short-circuit current among the devices are consistent with the difference in the thickness of the tritiated amorphous silicon layer. As the thickness of the tritiated layer is reduced, fewer beta-particles are created; hence, the number of electron–hole pairs created is reduced by nearly the same ratio. Since the structure of the delta devices is similar, the open-circuit voltages decrease monotonically with the short-circuit current. The open-circuit voltage of delta 3 did not decrease in comparison to delta 2. This is most likely the result of a better junction in delta 3. The smaller-than-expected short-circuit current from delta 3 is most likely due to a thinner-than-expected delta layer; the very short deposition time makes it difficult to accurately deposit the delta layer that was expected to be 300 Å thick.

For each device, the short-circuit current under dark conditions was measured as a function of time. The remaining fraction of the initial short-circuit current as a function of time is plotted in Fig. 11. After approximately 200 h, the short-circuit current for 'uniform' was less than 10% of its initial value. The decrease in the fractional short-circuit current for the delta-layered devices was not as rapid and, as can be seen in Fig. 11, the short-circuit currents appeared to settle asymptotically to a fractional value greater than that of 'uniform'. The short-circuit current for delta 3 decreased by only approximately 50% from its initial value after 600 h of operation. This difference in behaviour is because dangling bonds in the delta devices are isolated within a small, tritiated portion of the intrinsic region. Initially, in all the devices, there would have been a uniform electric field across the intrinsic region; however, as dangling bonds are created, the electric field weakens in

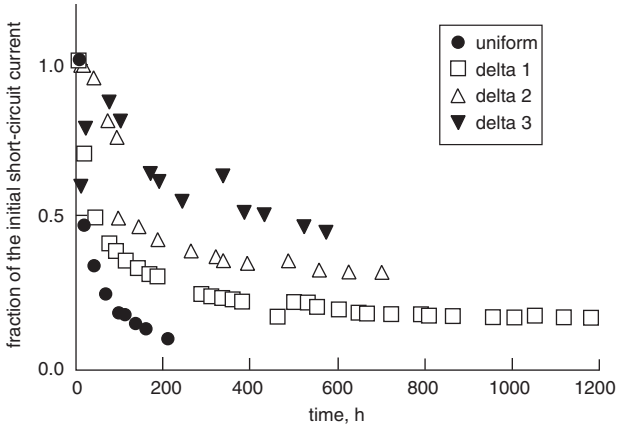

Fig. 11 *Short-circuit current as a function of time in p-i-n devices*

Table 5: Distribution of the beta-particle energy

Device	a-Si:H (top/bottom layer) % Energy (keV)				a-Si:H:T (delta layer) % Energy (keV)			
	1	2	3	5.7	1	2	3	5.7
delta 1	6.9	20	35	34	87	60	30	31
delta 2	13.7	36	43	40	36	27.4	15	19
delta 3	27.3	43.5	46	45	22.7	13	8.3	11

a-Si:H:T sections. In the device 'uniform', the electric field is weakened throughout most of the intrinsic region. In the delta devices, a weak electric field exists only in the delta layer. To accommodate the reduced electric field in the a-Si:H:T delta layer, the electric field strengthens in the a-Si:H region, increasing the drift velocity of carriers and helping carriers traverse the intrinsic region without recombination. This increased drift velocity in the untritiated region will have little effect, however, on the short-circuit current once the thickness of the tritiated region exceeds the diffusion length of the carriers.

A numerical simulation was carried out to determine the spatial distribution of the beta-particle energy deposited in the intrinsic regions as a function of the delta layer thickness, and the resulting initial short-circuit current [31]. The results of the simulations are summarised in Table 5. It can be seen that as the thickness of the a-Si:H:T region is reduced, increasingly more energy is deposited in the a-Si:H regions rather than in the a-Si:H:T region. This is to be expected since as the delta layer becomes thinner, relatively fewer electron–hole pairs are created in the a-Si:H:T region than in the a-Si:H region.

The energy transferred from a beta-particle to the amorphous silicon lattice is given by the stopping power of the material as the particle moves through the material. There is a broad distribution of kinetic energies of the beta-particles from the decay of tritium (Fig. 1). The initial kinetic energy of the beta-particle can be averaged between the most-probable energy of about 3 keV and the average energy of 5.7 keV. The energy deposited in each section of the intrinsic region was simulated using a uniform distribution of bonded tritium atoms and taking into account the path length travelled by the beta-particle as it loses energy to the lattice. The results of this calculation together with the corresponding experimental results are presented in Table 6. It can be seen that the numerical calculations agree quite well with the experimental data.

Table 6: Asymptotic value of the short-circuit current as a fraction of the initial short-circuit current for the three delta devices [31]

Device	Experiment	Numerical
delta 1	0.15	0.27
delta 2	0.30	0.36
delta 3	0.45	0.42

10 Conclusions

Tritium bonds stably in amorphous silicon. This is confirmed by outgassing, effusion, and infrared spectroscopy. The radioactive decay of tritium gives rise to the formation of dangling bonds as a consequence of tritium transmutation into helium; however, the number of dangling bonds appears to be much less than the number of decayed tritium atoms, most likely due to some form of lattice reconstruction.

Electron–hole pairs created by beta-particles emitted in the process of tritium decay are separated by the built-in field of a tritiated amorphous silicon p-i-n junction. Dangling bonds formed in the process of tritium decay cause degradation of the current–voltage characteristic of the p-i-n junction with time. This degradation can be controlled, however, by confining the tritium to small volumes in the p-i-n junction. Consequently, tritiated amorphous silicon may find an application in self-powered p-i-n junction betavoltaic batteries.

11 Acknowledgments

This work was supported by Ontario Power Technologies (now Kinectrics), Materials and Manufacturing Ontario, and Natural Sciences and Engineering Research Council of Canada.

12 References

1 Street, R.A.: 'Technology and applications of amorphous silicon' Springer Series in Materials Science', Vol. 37' (Springer, New York, 2000)
2 Bruno, G., Capezzuto, P., and Madan, A. (Eds.): 'Plasma deposition of amorphous silicon-based materials, Plasma–materials interactions' (Academic Press, Boston, 1995)
3 Street, R.A.: 'Hydrogenated amorphous silicon' (Cambridge University Press, Cambridge, UK, 1991), p. 203
4 Fuhs, W.: 'Electronic properties of amorphous silicon (a-Si:H)', in Kanicki, J. (Ed.): 'Amorphous and microcrystalline semiconductor devices' (Artech House, Boston, 1992), Vol. II, 1, pp. 1–53
5 Luft, W., and Tsuo, Y.S.: 'Hydrogenated amorphous silicon alloy deposition processes' Applied physics', Vol. 1 (Marcel Dekker, New York, 1993)
6 Vasaru, G.: 'Tritium isotope separation' (CRC Press, Boca Raton, FL, 1993)
7 Kherani, N.P.: 'Electron flux and energy distribution at the surface of lithium tritide'. PhD dissertation, Department of Physics, University of Toronto, Canada, 1994
8 Evans, R.D.: 'The atomic nucleus' (McGraw Hill, New York, USA, 1955) p. 625
9 Kherani, N.P., Kosteki, T., Zukotynski, S., and Shmayda, W.T.: 'Tritiated amorphous silicon for micropower applications', *Fusion Technol.*, 1995, **28**, (3), pp. 1609–1614
10 Kosteski, T., Kherani, N.P., Gaspari, F., Zukotynski, S., and Shmayda, W.T.: 'Tritiated amorphous silicon films and devices', *J. Vac. Sci. Technol. A, Vac. Surf. Films*, 1998, **16**, (2), pp. 893–896
11 Shmayda, W.T., Antoniazzi, A.B., and Surette, R.A.: 'Thermal desorption spectroscopy as an investigative technique for studying surface bound tritium'. Report no. 92-51-K. Ontario Hydro Research Division, Toronto, Canada, 1992
12 Stutzmann, M.: 'Data on hydrogen in a-Si:H from IR and Raman spectroscopy', in Searle, T. (Ed.): 'Properties of amorphous silicon and its alloys', EMIS Datareviews Series no. 19 (INSPEC, IEE, London, UK, 1998), pp. 56–60
13 Sidhu, L.S., Kosteki, T., Zukotynski, S., and Kherani, N.P.: 'Infrared vibration spectra of hydrogenated, deuterated, and tritiated amorphous silicon', *J. Appl. Phys.*, 1999, **85**, (5), pp. 2574–2578

14 Schneider, U., Schroder, B., and Finger, F.: 'Saturation effect and annealing behaviour of metastable defects induced by keV-electron irradiation in intrinsic a-Si:H', *J. Non-Cryst. Solids*, 1989, **114**, (Part 2), pp. 633–635
15 Stutzmann, M.: 'Metastability in amorphous and microcrystalline semiconductors', in Kanicki, J. (Ed.): 'Amorphous and microcrystalline semiconductor devices' (Artech House, Boston, , 1992), Vol. II, 4, pp. 129–187
16 Street, R., Biegelsen, D., and Stuke, J.: 'Defects in bombarded amorphous silicon', *Philos. Mag. B*, 1979, **40**, (6), pp. 451–464
17 Crandall, R.S.: 'Defect relaxation in amorphous silicon: stretched exponentials, the Meyer-Neldel rule, and the Staebler-Wronski effect', *Phys. Rev. B*, 1991, **43**, (5), pp. 4057–4070
18 Taylor, P.C.: 'Information on gap states in a-Si:H from ESR and LESR', in Searle, T. (Ed.): 'Properties of amorphous silicon and its alloys', EMIS Datareviews Series no. 19 (INSPEC, IEE, London, UK, 1998), Sec. 3.3, pp. 139–142
19 Staebler, D.L., and Wronski, C.R.: 'Reversible conductivity charges in discharge-produced amorphous Si', *Appl. Phys. Lett.*, 1977, **31**, (4), pp. 292–294
20 Stradins, P., and Fritzsche, H.: 'Photo-induced creation of metastable defects in a-Si:H at low temperature and their effect on the photoconductivity', *Philos. Mag. B*, 1994, **69**, (1), pp. 121–139
21 Zhang, Q., Takashima, H., Zhou, J.-H., Kumeda, M., and Shimizu, T.: 'Recovery process for light-soaked a-Si:H', in Schiff, E.A., Hack, M., Madan, A., Powell, M., and Matsuda, A. (Eds.): 'Symposium on Amorphous silicon technology – 1994' (Materials Research Society, Pittsburgh, PA, 1994), pp. 269–274
22 Tagliaferro, A.: 'A thermodynamic approach to stretched exponential relaxation', *Mod. Phys. Lett. B*, 1990, **4**, (22), pp. 1415–1419
23 Kakalios, J., Street, R.A., and Jackson, W.B.: 'Stretched-exponential relaxation arising from dispersive diffusion of hydrogen in amorphous silicon', *Phys. Rev. Lett.*, 1987, **59**, (9), pp. 1037–1040
24 Branz, H.M.: 'Hydrogen collision model: quantitative description of metastability in amorphous silicon', *Phys. Rev. B*, 1999, **59**, (8), pp. 5498–5512
25 Zhang, S.B., and Branz, H.M.: 'Hydrogen above saturation at silicon vacancies: H-pair reservoirs and metastability sites', *Phys. Rev. Lett.*, 2001, **87**, pp. 105503/1–4
26 Sidhu, L.S., Kosteki, T., Zukotynski, S., Kherani, N.P., and Shmayda, W.T.: 'Effect of dangling-bond density on luminescence in tritiated amorphous silicon', *Appl. Phys. Lett.*, 1999, **74**, (26), pp. 3975–3977
27 Street, R.A., and Biegelsen, D.K.: 'The spectroscopy of localized states', in Joannopoulos, J.D., and Lucovsky, G. (Eds.): 'Physics of hydrogenated amorphous silicon II. electronic and vibrational properties' (Springer-Verlag, Berlin, 1984), pp. 195–259
28 Chen, W.C., and Hamel, L.-A.: 'Monte Carlo simulation of transient currents in a-Si:H', in Hack, M., Schiff, E.A., Wagner, S., Schropp, R., and Mastsuda, A. (Eds.): 'Symposium on Amorphous Silicon Technology 1996' (Materials Research Society, Pittsburgh, PA, 1996), pp. 759–764
29 Wilson, B.A., Hu, P., Harbison, J.P., and JEDJU, T.M.: 'Sub-nanosecond total-light decay and spectra in *a*-Si:H', *Phys. Rev. Lett.*, 1983, **50**, (19), pp. 1490–1493
30 Lord, K.R., Walters, M.R., and Woodyard, J.R.: 'Investigation of the stability and 1.0 MeV proton radiation resistance of commercially produced hydrogenated amorphous silicon alloy solar cells'. Proc XIII Space Photovoltaic Research and Technology Conference, NASA Conference Publication 3278, 1994, (NASA Lewis Research Centre, Washington, DC), 187–197
31 Kosteski, T.: 'Tritiated amorphous silicon films and devices'. PhD dissertation, Department of Electrical and Computer Engineering, University of Toronto, Canada, 2001